Morphology and structure of ABS membranes filled with two different activated carbons

J. Marchese[a], M. Anson[a], N.A. Ochoa[a], P. Prádanos[b], L. Palacio[b], A. Hernández[b],*

[a]*Laboratorio de Ciencias de Superficie y Medios Porosos, Dpto. de Química, Facultad de Química-Bioquímica y Farmacia,
Universidad Nacional de San Luis, San Luis, Argentina*
[b]*Grupo de Superficies y Materiales Porosos, Dpto. de Física Aplicada, Facultad de Ciencias, Universidad de Valladolid, Valladolid, Spain*

Abstract

Mixed matrix-composite membranes (MMCM) for gas separation are prepared and characterized in this work. Acrylonitrile–butadiene–styrene (ABS) copolymer was used for the continuum phase of the membrane filled with two different activated carbons (AC). The so-obtained membranes have been characterized by gas permeability, optical microscopy, electronic microscopy and atomic force microscopy. The membranes have different roughness on both their surfaces but are always recovered by the polymeric material. Better ABS–AC adhesion has been always reached giving high selectivity and permeability for CO_2/CH_4. Such intimate contact can be attributed to the rubber properties of the butadiene–styrene chains in ABS. The morphological characteristics and the increase in both permeability and selectivity with the volume fraction of the filler are explained in terms of the properties of pure activated carbons.
© 2006 Elsevier Ltd. All rights reserved.

Keywords: Gas separation; Mixed matrix–composite membranes; Activated carbon; Membrane materials; Membrane characterization

1. Introduction

There is a big market for gas separation through membranes if materials structure and, thus, synthesis processes are considerably improved to reach the optimization of selectivity and permeability for target gases. Long-term research has been dedicated to this aim. Particularly, during last the two decades, two kinds of materials have been extensively studied: crosslinked polymers and mixed matrix materials (Koros and Mahajan, 2000). The Robeson equation (Robeson, 1991), gives an upper bound for the selectivity versus permeability correlation that can be reached by the increase in chain stiffness and/or frictional free volume. This limit is based on the empirical data for each given penetrant size ratio but seems to adapt well to a relatively simple model due to Freeman (1999). This lead to explore the possibility of combining polymers with other materials that should not be bound to the same selectivity versus permeation rules (Freeman, 1999). This should be the case not only with phase segregated block copolymers but also with the mixed matrix-composite membranes (MMCM).

The MMCM consist of two interpenetrated different materials and have potentialities linked with the easy processing and mechanical properties of the polymers and the good separation properties of rigid molecular sieving materials (te Hennepe, 1988; Süer et al., 1994; Vu et al., 2003a). A good selection of both the polymeric matrix and the inorganic filling material is crucial to obtain a good MMCM. Of course, the continuous and disperse phases should be chosen with a good adherence in order to avoid interfacial defects.

Simple models (Vu et al., 2003b), can predict permeabilities (and selectivities) of MMCM as a function of permeabilities of both disperse and continuous phases and the volume fraction of the disperse phase in the membrane. These models predict an increase in both permeability and selectivity when the volume fraction of the disperse phase increases. Nevertheless, sometimes they do not completely succeed to fit the experimental results. In many cases this mismatch could be attributed to the interactions between polymeric and disperse phases that these

---

* Corresponding author. Tel.: +34 983 423134.
   E-mail address: membrana@termo.uva.es (A. Hernández).

simple models do not take into account. Examples of these interactions are: clogging of the disperse phase by the polymer phase or modifications of the structure of polymer around the disperse phase inclusions (Moore and Koros, 2005). It is clear that a modification of interfacial regions should play a relevant role as far as the free volume of these interfaces should be different from those of each phase.

Inclusions should be distributed to allow a relevant portion of the permeant gas to cross the inorganic phase. This is why a close packing of the filler should enhance permeability and selectivity (Vu et al., 2003b). A configuration of filler particles forming layers of flakes should also be very adequate (Cussler, 1990).

Here, activated carbons (with high permeability and selectivity but with very inconvenient mechanic properties when used alone) are proposed as inorganic fillers in order to take profit of their different adsorption capacities for polar and unsaturated compounds against non-polar and saturated chemicals. As polymeric matrix ABS has been selected, as far as it is a copolymer, that combines the good selectivity of glassy polymers with high permeabilities of rubbery polymers (Marchese et al., 2003; Anson et al., 2004).

In this work, the structure of carbon aggregates, the distribution of smaller carbon particles inside the polymeric matrix and the subsequent modifications in the membrane morphology are analysed for different volume fractions of two activated carbons along with the resulting permeabilities and selectivities.

2. Experimental

2.1. Membrane materials

The polymeric matrix consisted in ABS, whose glass transition temperature is $110\,^\circ C$ with an approximated composition of: 60% styrene, 27% acrylonitrile and 13% butadiene as determined by FTIR with a Nicolet FTIR 5SxC (Marchese et al., 2003).

As inorganic fillers two activated carbons, hereafter called AC1 and AC2, were selected. The specific surface and pore size distributions of both the activated carbons used were analysed by the nitrogen adsorption technique with a Micromeritics ASAP 2010. Whereas their particle size distribution was determined by optical microscopy with a NanoScope OMV-PAL camera. The so-obtained characteristics of AC1 and AC2 are shown in Table 1. Note that, both the activated carbons have bimodal distributions but both have a very similar pore volume for pore sizes from 5 to 9 Å which is the relevant range for gas permeation. The pore size distributions are presented in Fig. 1.

2.2. Membrane preparation

Several proportions of activated carbons (2–10% w/w of AC1 and 20–40% w/w of AC2) were added to an ABS solution in Cl_2CH_2. The so obtained suspensions were casted at $25\,^\circ C$ in air (relative humidity of 45%) using a film extensor onto a glass plate. The resulting films were dried under vacuum at $80\,^\circ C$ during 48 h. Thus the resulting thickness ranged from 75

Table 1
Some characteristics of the activated carbons used

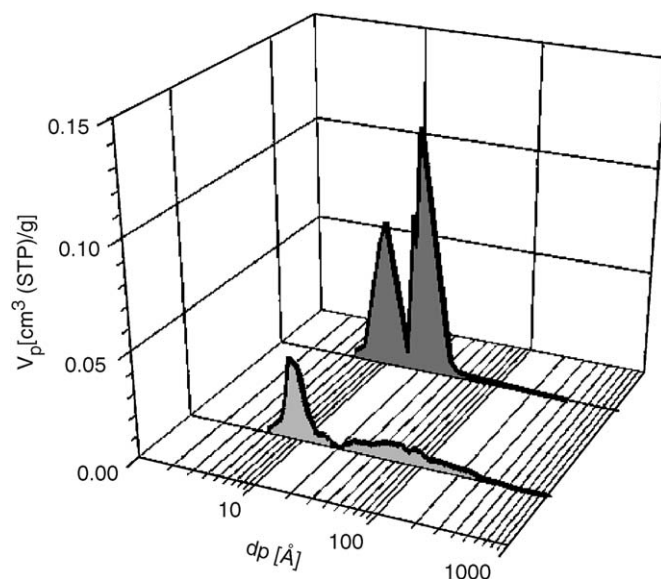|	AC1	AC2
BET surface, S_w (m^2/g)	3272	818
Monolayer capacity (BET), V_m (cm^3(STP)/g)	752	188
Apparent density, ρ_f (g/cm^3)	0.28	0.42
	Bimodal	Bimodal
Average pore size, d_p (å)	9.0 22.4	8.6 70.0
Mean particle size, d (µm)	0.90 ± 0.08	4.5 ± 2.8

Fig. 1. Pore size distribution for AC1 and AC2 obtained by the DFT method.

Table 2
Activated carbon composition of the MCMM

Carbon	MMCM	C (% w/w)	ϕ	A_{polym}/A_{total} (%)
AC1	M2	2	0.074	73
	M5	5	0.166	62
	M7	7	0.240	57
	M10	10	0.290	50
AC2	M20	20	0.388	52
	M25	25	0.456	50
	M33	33	0.552	41
	M40	40	0.624	32

The area occupied by carbon on the membrane surface for samples of a thickness of 25 µm is also shown.

to 125 µm. Some thinner membranes, 25 µm, have been manufactured to perform transmission optical microscopy through them. In Table 2 the volume fraction, ϕ, of each MCMM prepared is shown.

2.3. Membrane characterization

The topography of the membranes prepared has been studied by several microscopic techniques.

- Optical microscopy (OM) by using the NanoScope OMV-PAL camera: the samples were analysed attending to both transmitted and reflected light.
- Atomic force microscopy (AFM): pictures of both membrane sides were obtained to measure their roughness and to detect the presence of surface small pores. On the other hand, the membranes were embedded in an epoxidic matrix and cut with a microtome. The so-obtained transversal sections were also analysed with AFM to evaluate the distribution of small carbon particles into the polymeric matrix. All AFM measurements have been done with a Nanoscope IIIA from Digital Instruments by using the tapping mode. This intermittent-contact technique allows a simultaneous registration of the deflection and phase changes in the oscillation of the cantilever thus giving information on topography and viscoelastic properties of the surface to detect heterogeneities on the surface scanned by the tip.
- Environmental scanning electron microscopy (ESEM): samples were fractured in liquid N_2 and examined by using an accelerating voltage of 15 kV.

Image analysis was carried out by means of Jandel® ScanPro software (version 3.00.0030). Each photograph was digitized with a resolution of 1024×768 pixels, assigning to each one a grey level ranging from 0 (black) to 255 (white). Then, a clear-field equalization was applied to each image field to eliminate parasite changes in grey levels due to uneven bending or illumination. Once these effects were eliminated, the image grey spectrum was spanned to get the maximum contrast and definition. Then the images were redefined according to an assigned grey threshold level under which every pixel was assigned to 1 and the rest to 0. The resulting binary picture was improved by scraping isolated pixels, in such a way that all the remaining ones in the matrix were assumed to belong to the element being studied. Finally, borders were smoothed in order to reduce the influence of the finite size of pixels and low definition. Of course, a correct selection of grey threshold level is fundamental for correctly and accurately identifying grains or pores.

Customarily, the grey spectrum is analysed and the threshold centred in the peak-to-peak valley of the almost bimodal distributions is obtained.

The flux and permeability of the so-obtained MCMM were measured with a classical time lag method for both CO_2 and CH_4 pure gases.

3. Results and discussion

3.1. MMCM morphology and structure

3.1.1. Optical microscopy

In Fig. 2a–c, examples of the images obtained by OM with transmitted light are shown. When membranes with the same activated carbon (M2–M10 or M20–M50) are analysed, it is clear that the polymer area without carbon particles, decreases almost linearly for increasing activated carbon volume fractions. Of course, this coverage ratio depends on the membrane thickness, but for similar thickness it gives an idea of the amount of activated carbon that the gas crosses during permeation. The so-obtained percentage of carbon-free area is shown in Table 2, for 25 μm-thick membranes. In all cases the particles resulted to be are randomly distributed and an extrapolation to four times thick membranes should ensure that the gas should cross always some active carbon.

From an analysis of the picture presented in Fig. 2a, a distribution of activated carbon particles has been obtained as shown in Fig. 3. This distribution is bimodal. The small size peak (around 2-μm) should correspond to the original AC1 particles along with small agglomerates (see Table 1). Secondly, very low peak should correspond to big agglomerates of AC1 particles. This kind of analysis can be conducted only for the membranes containing low fractions of activated carbon, as far as in this case shadows should correspond to different particles or agglomerates.

Also in Fig. 2d and e, the reflected light images of a M20 membrane are shown. Both upper (d) and down sides (e) are shown. On the upper side (this is exposed to air during casting)
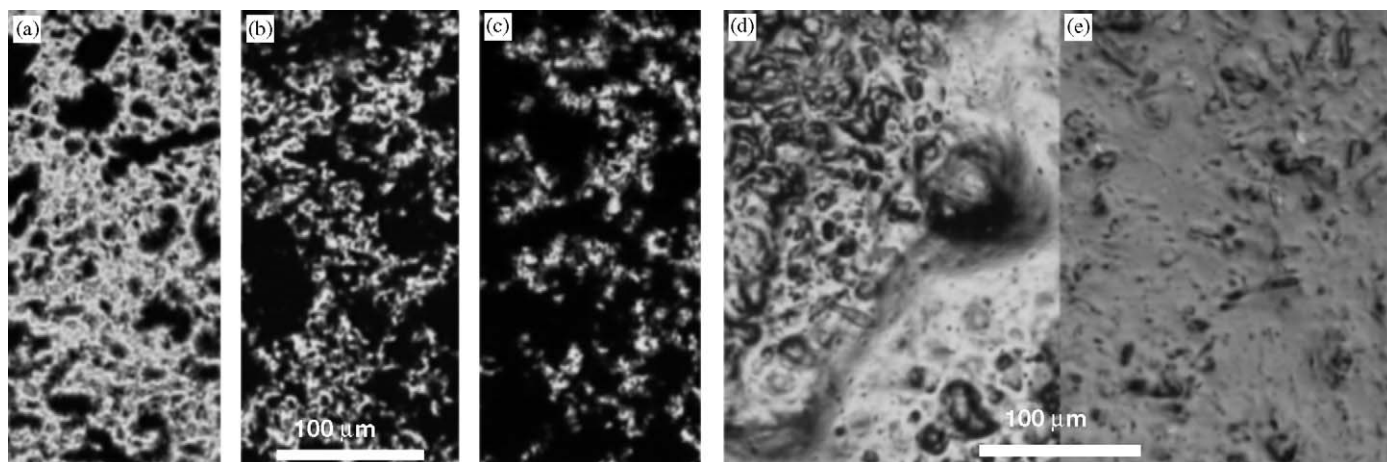

Fig. 2. Optical photographs. Transmitted light: (a) M2; (b) M5; (c) M7. Reflected light for a M20 membrane: (d) upper side; (e) down side.
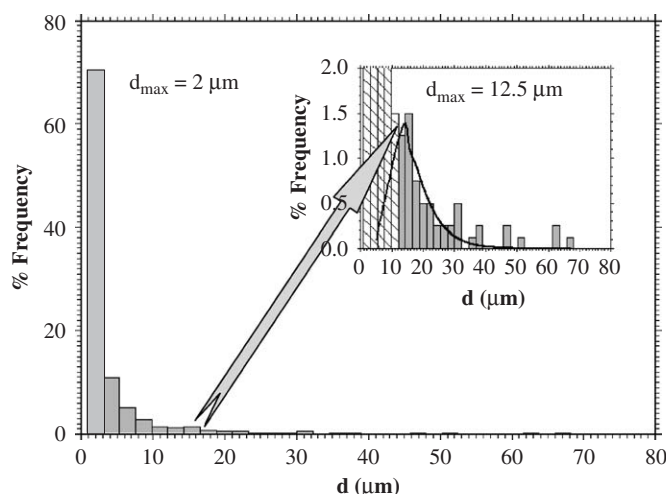
Fig. 3. Distribution of AC1 particles and agglomerates obtained by transmitted light optical microscopy for the M2 membrane.

extensive valleys can be seen. The area of the crests that defines these valleys increases with increasing filling volume fraction. Nevertheless, an in depth analysis of them will show (see below) that there is polymer on the top of them even if there are AC particles below them as should be reasonable. The down side, which remained in contact with the glass surface during casting, has much smoother surfaces.

3.1.2. Atomic force microscopy

Both sides of the membranes have been studied by AFM and areas from $50 \times 50\,\mu m$ to $0.5 \times 0.5\,\mu m$ have been scanned. As already seen in the reflected light OM images, AFM lead to roughness values, R_q, that are always higher for the upper side than for the down side. Moreover, R_q of both sides of the membrane increases with the content of active carbon when big areas are scanned. For the scanned areas below $2.5 \times 2.5\,\mu m$, roughness becomes independent of the AC content, which seems to confirm that over the activated carbon particles there is always a layer of polymer. This is also confirmed by the phase-contrast AFM that shows that no heterogeneous viscoelasticity can be detected on the membrane surfaces. The so reached constant roughness are: 6.40 nm for the upper side and 3.50 nm for the

down side of the membranes containing AC2 and 4.89 nm for the upper side and 3.65 nm for the down side of the membranes containing AC1.

The different roughness for both sides of each membrane can be attributed to the presence of pores from 40 to 150 nm that should be, probably, due to the evacuation of solvent and appear more frequently, as can be observed in Fig. 4, in the side opened to air during casting. The surface densities of these pores are: 4.64 pores/μm^2 in the upper side and 1.92 pores/μm^2 in the down side for AC2-containing membranes and 7.52 pores/μm^2 and 2.20 pores/μm^2, respectively, for the AC1-containing membranes. These pores appear more for AC1 membranes because AC1 has more porous volume (higher BET area and lower apparent density as can be seen in Table 1). They are purely superficial as otherwise permeability should be much higher than actually found and selectivity much lower. The roughness depends also on the size of the activated carbon particles, as far as AC1 has a mean diameter of $0.9\,\mu m$, whereas AC2 has a mean diameter of $4.4\,\mu m$.

Transversal sections show carbon particles and agglomerates from 1 to $30\,\mu m$ for AC1 membranes and 3 to $20\,\mu m$ for AC2 membranes, when the scanned big areas are studied. These sizes should correspond to aggregates up to 30 particles of AC1 and 5 particles of AC2. These sizes are in the OM range and compare well with those shown in Table 1 and Fig. 3.

In higher-resolution images, corresponding to small scanned areas, much smaller particles are revealed: ranging from 60 to 750 nm (with an average of 140 nm) for the membranes containing AC1 and from 60 and 900 nm (with an average of 300 nm) for those containing AC2. It is worth noting that also these small activated carbon particles are bigger for AC2 than for AC1 as is the case with those shown in Table 1.

The biggest agglomerates detected are visualized directly in topography due to the process of fracture, while the small particles were detectable by using the phase-contrast technique due to the different viscoelastic properties of the polymer matrix and the carbon inclusions. Examples of the corresponding AFM pictures are shown in Figs. 5 and 6. Higher carbon densities are found for AC2-containing membranes according to the data in Table 2.

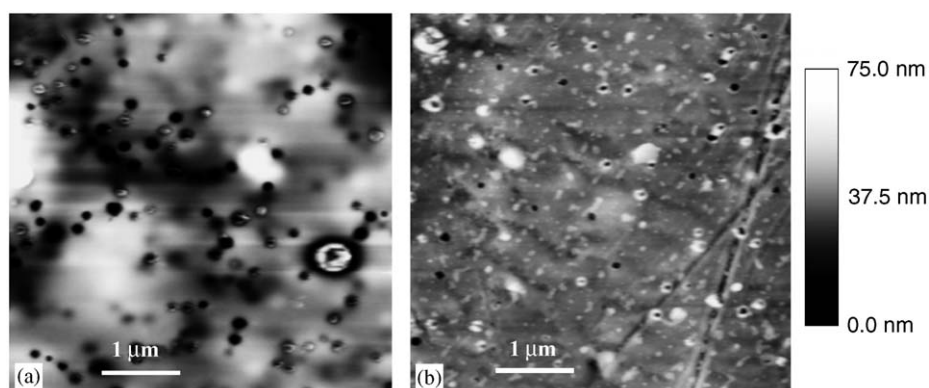In all cases transversal sections show always a good adherence and contact between the polymer continuous matrix

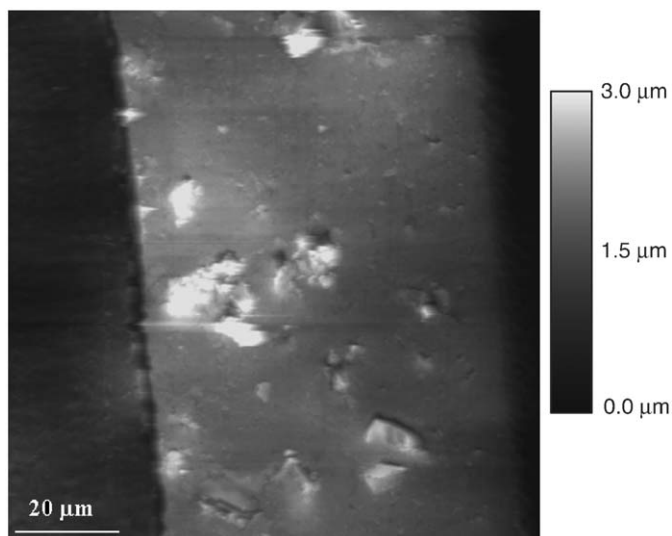Fig. 4. AFM images of M20 membrane: (a) up side; and (b) down side. $5 \times 5\,\mu m$ pictures are shown.

Fig. 5. AFM topographic image of a transversal cut of a M5 membrane. Clear peaks within the membrane are carbon grains. $100 \times 100 \, \mu m$ pictures are shown.

and the activated carbon particles. No changes in the viscoelastic properties of the polymeric phases in contact with carbon-disperse phase are seen.

3.1.3. Environmental electron scanning microscopy

Fig. 7a shows the representative ESEM images of transversal sections of the MMCM containing AC1. These pictures show AC1 clusters that are differently sized and randomly distributed through the membrane. No voids or deformations in the polymeric matrix are observed according to a good interfacial contact between inorganic and organic phases as already observed in the AFM pictures. These observable clusters range from 1 to 30 μm in size as already detected from the AFM pictures. Smaller active carbon particles have not been detected by this technique. For carbon mass percentages below 25%, the ESEM pictures of the MMCM containing AC2 have a very similar aspect to those containing AC1, with clusters in the range

from 3 to 20 μm (also agreeing with the ranges detected by AFM). Whereas for mass percentages of a 33%, and higher, carbon agglomerates seem to contact each other, as shown in Fig. 7b.

Note that AC1-containing membranes have more spherical aggregates than those containing AC2. This corresponds to many spherical particles of AC1 ($\sim$ 30) that should conform a somehow also spherical aggregate, while few spherical ($\sim$ 5) particles of AC2 should lead to much more angular shapes for their aggregates.

As mentioned, all the membranes show a high roughness that increases with increasing AC percentages. The surface not exposed to air during casting (directly in contact with the glass plate) has always a lower roughness. This is also confirmed by the ESEM pictures (Anson et al., 2004). It is important to remember that, as concluded from AFM analysis, on both sides of the membrane there is a continuous polymeric phase recovering activated carbon aggregates.

3.2. Permeability and selectivity

Effective CO_2 and CH_4 permeabilities were measured at 20 °C for pressures from 2×10^5 to 8×10^5 Pa, giving results totally independent of pressure. The constant permeability for very different pressures confirms that the membranes have neither cracks nor pinholes. The lack of these defects confirms a good contact between the organic and inorganic phases probably due to a partial compatibility of the styrene–butadiene chains and the activated carbon that should allow them for a strong interaction.

The average permeabilities along with the corresponding selectivities, defined as

$$\alpha_{CO_2-CH_4} = \frac{P_{CO_2}}{P_{CH_4}} \tag{1}$$

clearly increase with the content of the active carbon. Such tendencies are shown in Fig. 8 along with the corresponding Robeson upper bound (Robeson, 1991). According to the analysis of Moore and Koros (2005), such simultaneous increase of permeability and selectivity should correspond to an absence of
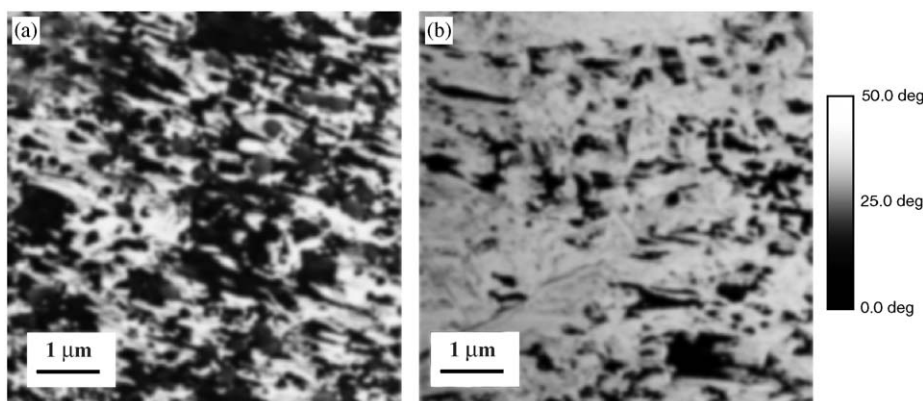

Fig. 6. Phase-contrast images of: (a) M5 membrane; (b) M20 membrane. Clearest areas are polymer, whereas dark spots correspond to the activated carbon particles. $5 \times 5 \, \mu m$ pictures are shown.
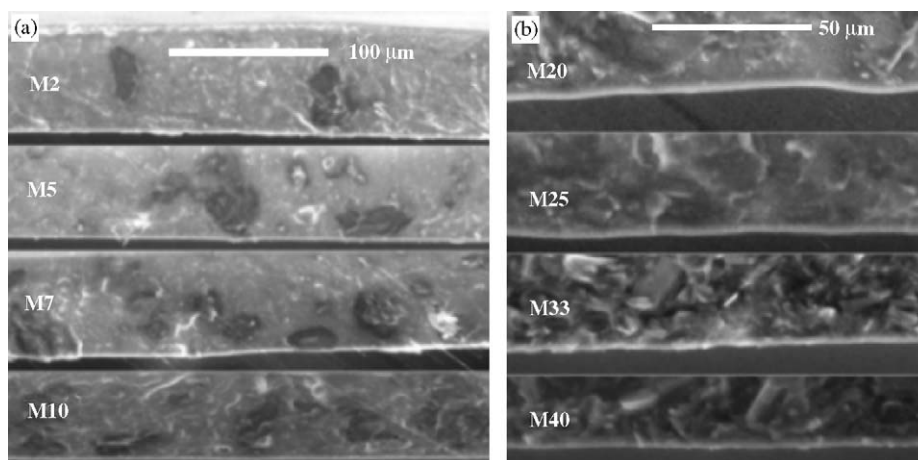
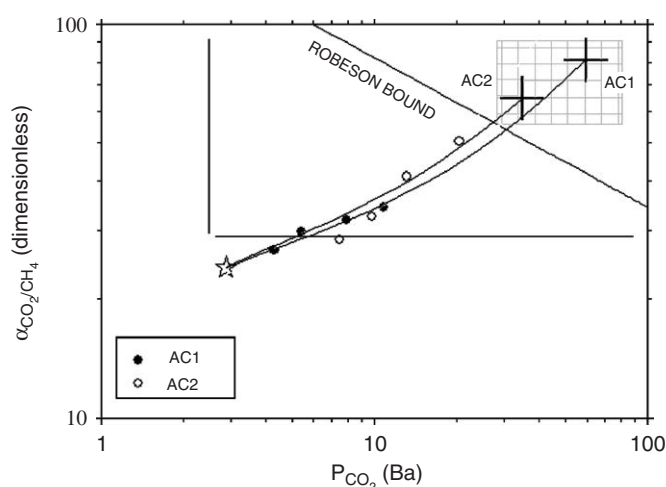Fig. 7. ESEM images of transversal sections of all membranes used: (a) with AC1; and (b) with AC2.

Fig. 8. Robeson diagram (selectivity versus permeability) corresponding to the MMCM studied and to the pair CO_2 and CH_4. The Robeson tradeoff line and the commercially attractive rectangle are also shown.

modifications of the polymer properties in the interface with the inorganic filler with no clogging of transport path though the filler particles and with a good adhesion filler–polymer. This good adhesion is compatible with the absence of voids around particle fillers seen in the SEM and AFM pictures.

If it is assumed that, in effect, there are no significant changes in permeabilities attributable to the interaction of the filler with the continuous polymeric phase. For a system where the filler is very close to a disposition of dispersed spheres, the theory of Maxwell can be applied to give

$$P_{i,\mathrm{mem}} = P_{i,c} \left[\frac{P_{i,d} + 2P_{i,c} - 2\phi(P_{i,c} - P_{i,d})}{P_{i,d} + 2P_{i,c} + \phi(P_{i,c} - P_{i,d})} \right] \qquad (2)$$

for the permeability of the membrane (MMCM) for the ith gas and with d and c subindexes referring to disperse (filler) and continuous (polymer) phases (Vu et al., 2003b; Robeson et al., 1973; Zimmerman et al., 1997). This of course can be used to fit experimental results on permeability and selectivity to predict

the permeability and selectivity of pure activated carbon from those corresponding to different volume fraction of activated carbons. The corresponding results are shown in Fig. 8. Fitting has been done by highly overweighting the low volume fraction experimental results according to the conditions of applicability of the simple Maxwell theory (Gonzo et al., 2006).

As can be seen, membranes containing only AC1 should be better than those with only AC2 (extrapolated pure AC1 and AC2 points in Fig. 8). This should be due to the better selectivity of AC1, due to the high population of narrower pores (low pore size peak in the pore size distribution) that the AC1 particles have, along with an also high population of the wider pores they present (high pore size peak in the pore size distribution) that should lead to a higher permeability (Fig. 1). This difference in selectivities can also be attributed to the higher BET area of AC1 over AC2 as shown in Table 1. Given that narrow pores are similar in size for both the active carbons, it is probable that higher selectivities should be mainly attributable to CO_2 adsorption that should clearly be much higher for AC1-containing MMCM.

Nevertheless, it is important to take into account that for the mechanically sure range of volume fractions, that comprises approximately the volume fractions used here, the membranes containing AC2 are better as far as higher volume fractions are attainable for them. Although the MMC membranes did not exceed the Robeson upper bound, they displayed improved performances within the attractive region (Koros and Mahajan, 2000).

4. Conclusions

OM shows that, in the MMCM including activated carbon, a random agglomeration of carbon particles appear. The surface morphology of these membranes differs from side to side.

The atomic force analysis allowed to measure the roughness whose small differences, from side to side and different activated carbon particles have been explained in terms of the manufacture process. In any case, both sides are covered by

the polymer. Some surface bottle ink pores have been also detected by AFM, these craters can be attributed to the elimination of solvent trapped in the activated carbon pores. There is a good adhesion between both the continuous and disperse phases without a detectable modification of the interfacial area.

The ESEM of transversal sections of MMCM confirms most of the features analysed by OM and AFM, and particularly the presence of activated carbon agglomerates randomly distributed inside and with an intimate contact with the polymeric matrix.

The permeability and selectivity of the hypothetical pure carbon membranes have been extrapolated by using the very simple model of Maxwell. In this model no relevant modifications in the disperse–continuous phase interface are assumed with no clogging of the disperse phase pores and with a good adherence between both the phases, which seems to be confirmed by the simultaneous increase of selectivity and permeability with increasing volume fraction of activated carbon.

Other more exact models (Gonzo et al., 2006; Moore et al., 2004) are too complex to allow a good fitting to the experimental results. In any case, the Maxwell model has been used by forcing fitting to adapt better to the low volume fraction data, in the range were the Maxwell model is relatively sure (Gonzo et al., 2006). In any case, these extrapolated values for AC1 and AC2 should be taken as only rough estimations, mainly usable to compare each other.

The higher BET area and porous volume for small enough pore sizes of AC1 over AC2 has observable effects in the morphology of the MMCM membranes and explains the better separation and permeability of the membranes including AC1 for similar volume fractions.

The high performances of these MMCM made from ABS–carbon (good permeability and selectivity for CO_2/CH_4) indicate that the pores detected by AFM do not cross the membranes and, once again, that there is a good adhesion of activated carbon with the ABS matrix.

The MMC membranes obtained by including activated carbon particles in the ABS matrix did not cross the tradeoff line but entered well in the commercially attractive selectivity versus permeability characteristics.

Acknowledgements

References

Anson, M., Marchese, J., Garis, E., Ochoa, N.A., Pagliero, C., 2004. ABS copolymer-activated carbon mixed matrix membranes for CO_2/CH_4 separation. Journal of Membrane Science 243, 19–28.

Cussler, E., 1990. Membranes containing selective flakes. Journal of Membrane Science 52, 275.

Freeman, B.D., 1999. Basics of permeability/selectivity tradeoff relations in polymeric gas separation membranes. Macromolecules 32, 375–380.

Gonzo, E.E., Parentis, M.L., Gottifredi, J.C., 2006. Estimating models for predicting effective permeability of mixed matrix membranes. Journal of Membrane Science 277, 46–54.

te Hennepe, H.J.C., 1988. Zeolite filled polymeric membranes: a new concept in separation science. Thesis, University of Twente.

Koros, W.J., Mahajan, R., 2000. Pushing the limits on possibilities for large scale gas separation: which strategies? Journal of Membrane Science 175, 181–196.

Marchese, J., Garis, E., Anson, M., Ochoa, N.A., Pagliero, C., 2003. Gas sorption, permeation, and separation of ABS copolymer membrane. Journal of Membrane Science 221, 185–197.

Moore, T.T., Koros, W.J., 2005. Non-ideal effects in inorganic–inorganic materials for gas separation membranes. Journal of Molecular Structure 739, 87–98.

Moore, T.T., Mahajan, R., Vu, D.Q., Koros, W.J., 2004. Hybrid membrane materials comprising organic polymers with rigid dispersed phases. A.I.Ch.E. Journal 50, 311–321.

Robeson, L.M., 1991. Correlation of separation factor versus permeability for polymeric membranes. Journal of Membrane Science 62, 165–185.

Robeson, L.M., Noshay, A., Matzner, M., Merrian, C.N., 1973. Physical property characteristics of polysulfone/poly-(dimethylsiloxane) block copolymer. Angewandte Makromoletylene Chemie 29/30, 47–62.

Süer, M.G., Baç, N., Yilmaz, L., 1994. Gas separation characteristics of polymer–zeolite mixed matrix membranes. Journal of Membrane Science 91, 77–86.

Vu, D.Q., Koros, W.J., Miller, S.J., 2003a. Mixed matrix membranes using carbon molecular sieves I. Preparation and experimental results. Journal of Membrane Science 211, 311–334.

Vu, D.Q., Koros, W.J., Miller, S.J., 2003b. Mixed matrix membranes using carbon molecular sieves II. Modeling permeation behaviour. Journal of Membrane Science 211, 335–348.

Zimmerman, C., Singh, A., Koros, W.J., 1997. Tailoring mixed matrix composite membranes for gas separations. Journal of Membrane Science 137, 145–154.